INTERACTION OF HEAT RELEASE AND TURBULENCE IN THE REACTING SHEAR LAYER

Carlos Pantano
Mechanical and Aerospace Engineering
University of California at San Diego
La Jolla, CA 92093
cpantano@mae.ucsd.edu

Sutanu Sarkar
Mechanical and Aerospace Engineering
University of California at San Diego
La Jolla, CA 92093
ssarkar@ucsd.edu

ABSTRACT

Direct numerical simulations (DNS) of a reacting shear layer with large heat release characteristic of hydrocarbon combustion are performed. It is found that strong heat release leads to substantial modifications in the shear layer growth rate as well as turbulence statistics.

INTRODUCTION

The interaction of heat release and turbulence is of interest in technological applications such as combustion, high-speed propulsion and energetic devices. The reacting shear layer is a prototypical example to study such interactions. Previous experimental studies on the reacting shear layer have been performed by Wallace (1981), Mungal and Dimotakis (1984), Hermanson and Dimotakis (1989), and Miller, Bowman and Mungal (1998). With the exception of a case with convective Mach number, $M_c = 0.7$, studied by Miller *et al.*, these experiments consider low-speed flows. Salient results, generally representative of all the experiments, are summarized below. The vorticity thickness growth rate of the shear layer is observed to decrease somewhat with heat release. For example, Hermanson and Dimotakis (1989) report an approximately 15% reduction at the highest heat release rate with corresponding temperature change, $T_{max}/T_0 = 4$. The volumetric entrainment rate is found to be substantially reduced essentially because higher-density ambient fluid is entrained into the mixing layer whose density is reduced due to heat release. The turbulent momentum transport, $\bar{\rho}R_{12}$, was found to decrease substantially with heat release. Although most of the decrease was attributed to reduced mean density $\bar{\rho}$, some changes in the shear stress R_{12} were inferred.

DNS studies of the reacting shear layer have been conducted by McMurtry, Riley and Metcalfe (1989), and Miller, Madnia and Givi (1994). The former considered moderate heat release, $T_{max}/T_0 = 2$, while the latter considered low heat release, $T_{max}/T_0 = 1.2$. A reduction in growth rates consistent with the experimental observations was observed in these studies.

The objective of the current DNS study is to consider large heat release rates typical of hydrocarbon combustion ($T_{max}/T_0 \simeq 8$) and study not only the overall growth characteristics but also the turbulence structure. Observations regarding the growth rate, all components of the Reynolds stress tensor, and the turbulent dissipation rate, and the r.m.s thermodynamic variables are documented. In addition, the changes in the growth rate are analytically linked to the mean density field.

PROBLEM DESCRIPTION

Formulation

Non-premixed combustion in a shear layer between methane and air streams is considered. Although simulations have been conducted over a wide range of Mach numbers, the current contribution focuses on the effect of heat release in the low-speed regime with

convective Mach number, $M_c = 0.3$.

A simple chemistry model is sufficient to capture the leading-order effect of heat release on the flow evolution. In the present study, single-step, infinitely-fast irreversible chemistry is assumed,

$$CH_4 + 2O_2 \rightarrow CO_2 + 2H_2O \qquad (1)$$

The stoichiometric mixture fraction value, $\zeta_s = 0.2$, is fixed by diluting the fuel stream with N_2. This gives an equivalence ratio of $\phi = 2$. Realistic values are used for all thermochemical properties. Heat release introduces an additional parameter

$$Ce = \frac{\Delta h^o Y_{f,-\infty}}{C_{po} T_o (1+\phi)} \qquad (2)$$

which can be related to the adiabatic flame temperature by $Ce = T_{ad} - 1$ where T_{ad} is the normalized adiabatic flame temperature in the case of constant C_p. The molecular viscosity, μ, the mixture fraction diffusivity, ρD, and the thermal conductivity κ are taken as constants and, furthermore, the Prandtl and Schmidt numbers are fixed to be $Pr = Sc = 0.7$.

Under the assumptions of infinitely-fast chemistry, a single conserved-scalar equation for the mixture fraction, ζ, is sufficient to describe the chemical system,

$$\frac{\partial(\rho\zeta)}{\partial t} + \frac{\partial(\rho\zeta u_k)}{\partial x_k} = \frac{1}{ReSc}\frac{\partial}{\partial x_k}\left(\rho D \frac{\partial \zeta}{\partial x_k}\right) \qquad (3)$$

Although the species mass fractions, Y_i, are prescribed algebraic functions of ζ, the temperature is not, ie; $T \neq T(Z)$. Unlike the low Mach number formulation, the energy conservation equation is explicitly solved in our extension of the Burke-Schumann formulation to compressible flows.

Numerical method

The problem formulation leads to an unsteady, three-dimensional system of equations which governs the evolution of the three velocity components, density, energy and the mixture fraction. The transport equations are integrated using a 6th order of accuracy compact Padé scheme in space. The time advancement is performed with a fourth order of accuracy low storage Runge-Kutta scheme. Periodic boundary conditions in streamwise (x_1) and spanwise (x_3) directions are used and 'non-reflective' boundary conditions are imposed in the cross-stream (x_2) direction. A uniform grid is used.

Description of the simulations

Computations are performed with grids as large as 256x192x128 and with large evolution times, required to achieve full-blown turbulence. The Reynolds numbers based on vorticity thickness are of the order of 8000 for the different simulations and broadband fluctuations are imposed at $t = 0$ to accelerate transition. The microscale Reynolds number, $Re_\lambda \simeq 100$. The stoichiometric mixture fraction is $\zeta_{st} = 0.2$ with free stream values of $\zeta = 0$ in the upper air stream and $\zeta = 1$ in the lower methane stream, respectively. The heat release is parametrized by Ce defined by Eq. (2). High-speed effects are parametrized by the convective Mach number, defined as $M_c = (U_1 - U_2)/(c_1 + c_2)$, where the velocity, density and speed of sound in stream i are U_i, ρ_i, and c_i. Any difference in free-stream states is characterized by the density ratio, $s = \rho_2/\rho_1$.

In the following discussion of results, we will focus primarily on the effect of heat release in the low-speed regime, $M_c = 0.3$. Three cases will be discussed in detail: a cold, nonreacting case C3 with $Ce = 0$, a hot, reacting case H3 with $Ce = 7.0$, and a reacting case CH3 with $Ce = 3.5$ corresponding to intermediate heat release.

THE DENSITY FIELD

A longitudinal snapshot of the density field is shown in Fig. 1. The upper air stream moves to the left with velocity $-\Delta U/2$ while the lower fuel stream moves to the right with velocity $\Delta U/2$. The stoichiometric mixture fraction is $\zeta = 0.2$; the *mean* location of the flame sheet is displaced upwards to the air side at $y = 15.28 = 0.31\delta_\omega$ in the figure. However, the convective stirring of the flame sheet by the turbulent motion spans the entire width of the shear layer so that an instantaneous snapshot such as Fig. 1 shows a *wide* central core of hot, low-density fluid separated from the cold, high-density fluid on either side by thin regions with large values of the density gradient.

Figure 2 shows the average density for the different simulations as a function of the self-similar coordinate, η. The length scale used in the definition of the self-similar coordinate is the vorticity thickness, giving $\eta_\omega = x_2/\delta_\omega$, and δ_ω is defined as

$$\delta_\omega = \frac{\Delta u}{\left|\frac{\partial \tilde{u}_1}{\partial x_2}\right|_{max}} \qquad (4)$$

Favre averages are used to calculate the aver-

Ce	$\bar{\rho}_{min}$	$\dot{\delta}_\theta$	$\dot{\delta}_\theta/\bar{\rho}_{min}$
0.0	1.0	0.015	0.015
3.5	0.35	0.0047	0.0134
7.0	0.22	0.0031	0.0141

Table 1: Normalized momentum thickness growth for $M_c = 0.3$ and various Ce.

age velocity in this definition. Figure 2 shows that the minimum density reaches 0.35 for $Ce = 3.5$ and 0.22 for $Ce = 7$. The location of the minimum mean density is coincident with that of the mean flame location, ie; the position where $\bar{\zeta} = \zeta_s = 0.2$. The mean density profile is somewhat flat near its minimum value corresponding to the central region of well-mixed, high-temperature fluid seen in the instantaneous snapshot, Fig. 1.

THICKNESS GROWTH RATE

An important aspect from the application point of view is the effect of heat release on the growth rate of the mixing layer. Previous experimental measurements have found that heat release reduces the growth rate of the shear layer. Although, in the experimental measurements, the levels of heat release were smaller that the ones used here, the trend observed in the current DNS is the same.

The momentum thickness defined by

$$\delta_\theta = \frac{1}{\rho_o \Delta u^2} \int_{-\infty}^{\infty} \bar{\rho}\left(\frac{\Delta u}{2} - \tilde{u}_1\right)\left(\frac{\Delta u}{2} + \tilde{u}_1\right) dx_2 \,. \tag{5}$$

and the vorticity thickness, defined by Eq. (4), are popular measures of the shear layer thickness. It is important to distinguish between these two thickness measures when studying the influence of heat release.

Table 1 shows the momentum thickness growth rate and the result of normalizing this value by the minimum average density. Column 3 of the table shows that there is a strong decrease of momentum thickness growth rate with increasing heat release. Column 4 of the table shows that most of this decrease of $\dot{\delta}_\theta$ is due to the reduction in the average density. This argument is only approximate since the effect of the density is not uniform in Eq. (5) but occurs through an integral. Moreover, the small extra reduction that accounts for approximately 10% of the total reduction is related to the Reynolds shear stress reduction, see figure 4.

The vorticity thickness growth rate also reduces with increasing heat release as shown by the fifth column of Table 2. An analysis to understand this trend has been carried out with

Ce	α_ω	$\tilde{R}_{12}$	$\tilde{R}''_{12}$	$\dot{\delta}_\omega/\dot{\delta}_{\omega,0}$	$\dot{\delta}_\omega/\dot{\delta}_{\omega,0}$, Eq. (6)
0.0	0.0	0.0115	-0.116	1.0	1.0
3.5	1.0	0.0084	-0.095	0.69	0.74
7.0	3.5	0.0080	-0.087	0.62	0.51

Table 2: Variation of terms in Eq. (6). $\dot{\delta}_{\omega,0}$ is the zero heat release value.

details provided by Pantano (2000); the final result is as follows,

$$\dot{\delta}_\omega = \left| \alpha_\omega R_{12} + \frac{d^2 R_{12}}{d\eta_\omega^2} \right|_c \tag{6}$$

where

$$\alpha_\omega = \left(\frac{1}{\hat{\rho}} \frac{d^2\hat{\rho}}{d\eta_\omega^2} - 2\left(\frac{1}{\hat{\rho}} \frac{d\hat{\rho}}{d\eta_\omega} \right)^2 \right) \tag{7}$$

Eq. (6) has a number of interesting implications. First, in the constant-density case, α_ω is identically zero, and the growth rate is directly related to the curvature of the Reynolds shear stress profile at the centerline. Second, when the density is nonuniform it is the shape of the mean density profile at the centerline rather than its magnitude that influences the vorticity thickness growth rate. Therefore, the vorticity thickness growth rate can be expected to be sensitive to free stream conditions such as the density ratio, s. Third, it is possible to explain the observed trend of a systematic decrease of $\dot{\delta}_\omega$ with increasing heat release as follows. In the reacting case, $d^2\hat{\rho}/d\eta_\omega^2|_c > 0$ while $d\hat{\rho}/d\eta_\omega|_c$ is small, see figure 2. Therefore, $\alpha_\omega > 0$. Irrespective of whether the high-speed stream is the lower or upper one, the sign of R_{12} and $d^2R_{12}/d\eta_\omega^2$ are opposite. Therefore, according to Eq. (6), heat release always causes a reduction in the shear layer thickness growth rate if both free streams have the same density.

The various terms of Eq. (6) are also given in Table 2. It can be seen that Eq. (6) captures the observed influence of heat release on the vorticity thickness growth rate. Some deviation between the calculated and measured growth rate is observed. This discrepancy can be attributed to the difficulty of accurately measuring the Reynolds shear stress curvature needed in Eq.(6).

We have performed simulations for both reacting and nonreacting cases over a wide range of Mach numbers. Fig. 3 is a composite plot that shows the growth rate for all the simulations with equal freestream densities, $s = 1$. With increasing values of M_c, the growth rate of the nonreacting DNS cases shows the well-known large reduction in agreement with the

Langley experimental curve. What is perhaps less expected is the effect of M_c on the growth rate of the reacting cases. The vorticity thickness growth rate is already quite low in the $M_c = 0.3$ reacting case and, although a further increase in M_c causes an additional reduction, it is not as dramatic as in the nonreacting cases. The figure also illustrates that distinction must be drawn between the momentum and vorticity thickness growth rates since the effect of heat release is substantially larger when the former is considered. In the case of nonreacting cases, no such distinction is required.

REYNOLDS STRESSES

It is theoretically expected that turbulence statistics in the shear layer such as Reynolds stress profiles collapse to a single profile when plotted in selfsimilar coordinates. According to the DNS results, the width of the profiles of the Reynolds stresses (and other statistics) scale well with the vorticity thickness but not the momentum thickness. Therefore, the vorticity thickness is henceforth used as the characteristic cross-stream scale for normalization.

Fig. 4 shows that there is a decrease of approximately 20% in the peak value of the Reynolds shear stress. There is a decrease of similar magnitude in the peak value of the streamwise component, R_{11} (not plotted). The cross-stream component also decreases with increasing heat release with an approximately 45% decrease at $Ce = 7$, with respect to the nonreacting case.

THE DISSIPATION RATE

In the nonreacting shear layer, the turbulent dissipation rate, ϵ, when normalized with $\Delta U^3/\delta_\omega$, eventually approaches a selfsimilar profile as expected from inviscid, outer scaling of the dissipation rate. It is of interest to find out if a similar scaling applies in the reacting case. The DNS results show that, after an initial transient, profiles of ϵ normalized using outer scaling tend to collapse. Fig. 6 shows that, with respect to the baseline nonreacting case, the peak value of the normalized turbulent dissipation rate changes by less than 10% and, the profile is also somewhat narrower.

The mean scalar dissipation has units of inverse time and provides a characteristic rate of mixing by turbulence. Similar to the turbulent dissipation rate, outer inviscid scaling works in the case of the scalar dissipation rate. DNS profiles (not shown here) provide an estimate for the mixing rate useful for simple models of turbulent combustion in a shear layer, namely, $\chi_{max} \approx 0.008\Delta u/\delta_\omega$.

THERMODYNAMIC FLUCTUATIONS

The behavior of the density, temperature and pressure fluctuations is shown in figures 7, 8 and 9 respectively. Reference quantities are used for normalization of the r.m.s. values. The other curves correspond to various reacting cases. The first thing that can be observed is that the level of fluctuations is very small in the non-reactive case for the density and the temperature in comparison with the reactive cases. The density fluctuation profiles in the reacting cases have two peaks at approximately $\eta = \pm 0.6$. These peaks are associated with the mixing that takes place between the light (hot) central region of the shear layer and the heavy (cold) free streams. It can also be seen that the peak at $\eta = x_2/\delta_\omega = 0.6$ is larger since the chemical reaction takes place closer to the upper stream ($\zeta_s = 0.2$). The peaks associated with mixing of reacting and non-reacting fluids ($\eta \approx 0.6$) near the average location of the flame sheet is present in both temperature and density profiles. However, the mixing of hot reacting fluid and the cold lower stream that leads to a sharp peak ($\eta \approx -0.6$) in the density profile leads to a plateau in the profile of r.m.s. temperature. Thus, the mixing of thermodynamic fluctuations is not a constant-pressure process with $\rho'/\rho \approx -T'/T$.

Profiles of the pressure r.m.s., normalized by the reference pressure, are shown in Fig. 9. As expected for a case with low Mach number, the normalized r.m.s. pressure is much smaller than corresponding values for the density and temperature. The peak value of r.m.s pressure is largest for the non-reactive case, $Ce = 0$, with lower values with increasing Ce. This reduction is presumably because the dynamic pressure, $\bar{\rho}K$, decreases along with the mean density in the presence of heat release.

CONCLUSIONS

DNS of a reacting shear layer with infinitely-fast chemistry has been performed with large temperature changes ($T_{max}/T_0 \approx 8$) to investigate modifications to the flow in response to heat release. Strong turbulent stirring and mixing in the core of the shear layer is reflected in instantaneous visualizations as well as the mean temperature and density profiles.

At the highest heat release, $Ce = 7$, the vorticity thickness growth rate decreases by approximately 40% while the momentum thickness is reduced even more. All components of the Reynolds stress tensor decrease with disproportionately larger decrease in the cross-stream component. The turbulent dissipation rate and scalar dissipation rate follow the inviscid, outer scaling expected for high-Reynolds number incompressible flow with somewhat smaller normalized values in the reacting cases. Overall, it appears that large heat release leads to substantial quantitative changes in the evolution of the velocity and associated statistics.

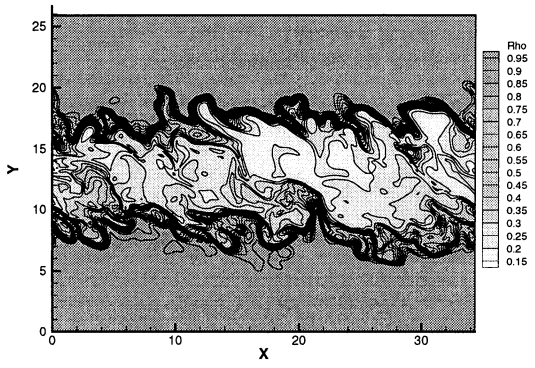

Figure 1: Instantaneous density visualization in a longitudinal plane

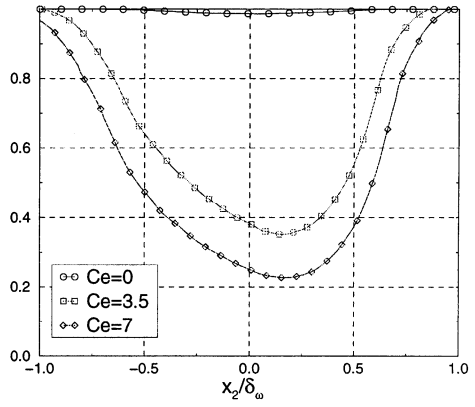

Figure 2: The mean density profile

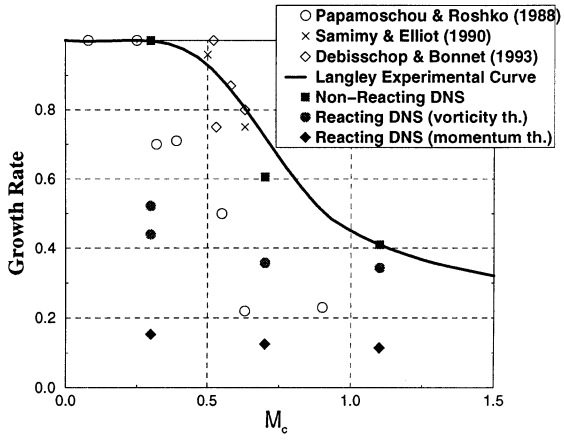

Figure 3: Effect of M_c on normalized growth rate.

References

Hermanson, J. C. and Dimotakis, P. E., 1989, " Effects of heat release in a turbulent, reacting shear layer," *J. Fluid Mech.*, **199**, 333-375.

McMurtry, P. A., Riley, J. J., and Metcalfe, R. W., 1989, " Effects of heat release on the large-scale structure in turbulent mixing layers," *J. Fluid Mech.*, **199**, 297-332.

Miller, M. F., Bowman, C. T., and Mungal, M. G., 1998, " An experimental investigation of the effects of compressibility on a turbulent mixing layer," *J. Fluid Mech.*, **356**, 25-64.

Miller, R. S., Madnia, C. K., Givi, P., 1994, "Structure of a turbulent reacting mixing layer," *Combust. Sci. and Tech.*, 1994, **99**, 1-36.

Mungal, M. G., and Dimotakis, P. E, 1984, " Mixing and combustion with low heat release in a turbulent shear layer," *J. Fluid Mech.*, **148**, 349-382.

Pantano, C., 2000, "Compressibility effects in turbulent non-premixed reacting shear flows," *Ph. D. thesis*, UC San Diego.

Pantano, C., and Sarkar, S., 2000, "A study of compressibility effects in the high-speed, turbulent shear layer using direct simulation, " *J. Fluid Mech.*, submitted.

Wallace, A. K., 1981, "Experimental investigation of the effects of chemical heat release in the reacting turbulent plane shear layer," *Ph. D. thesis*, University of Adelaide.

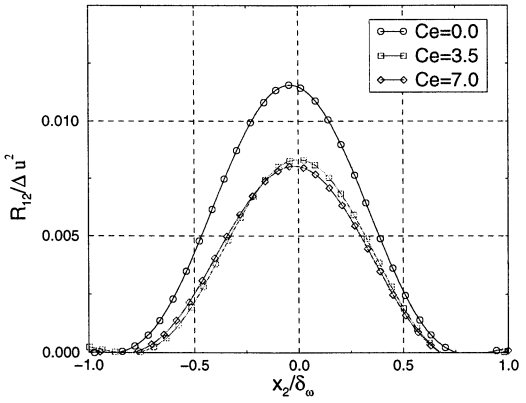

Figure 4: Reynolds shear stress profile; effect of Ce.

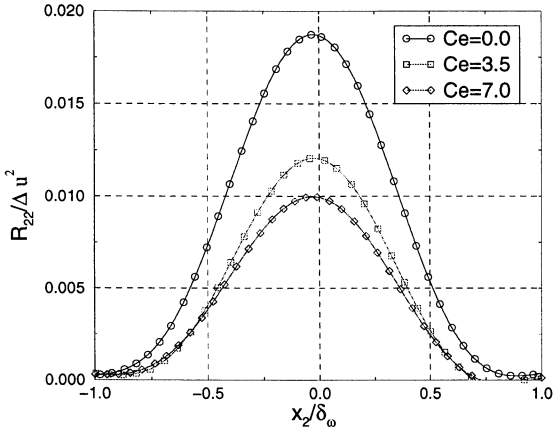

Figure 5: Profile of cross-stream turbulence intensity; effect of Ce.

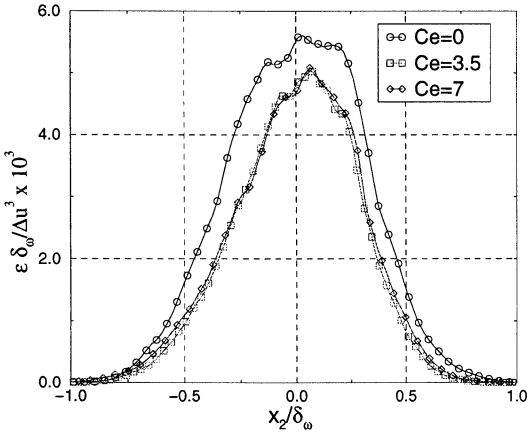

Figure 6: Normalized turbulent dissipation at different heat release and $M_c = 0.3$, $s = 1$.

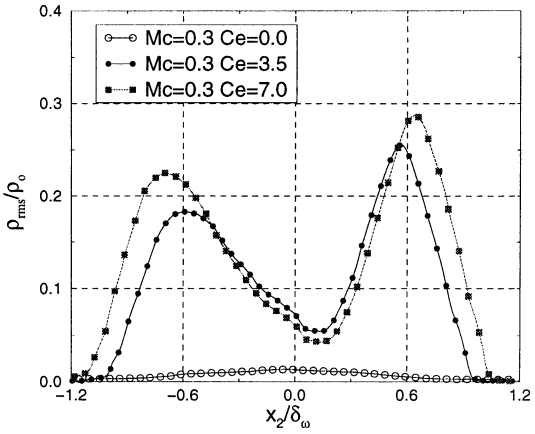

Figure 7: Density r.m.s. for different cases of heat release.

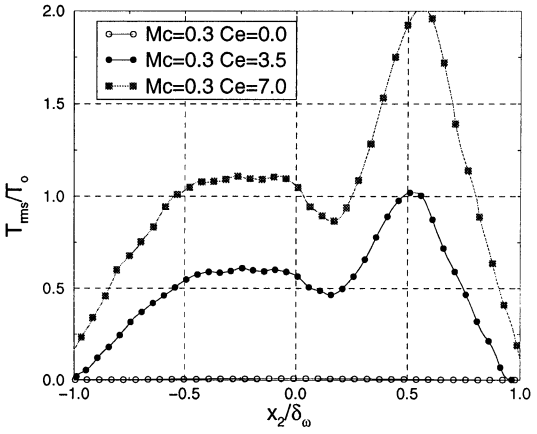

Figure 8: Temperature r.m.s. for different cases of heat release.

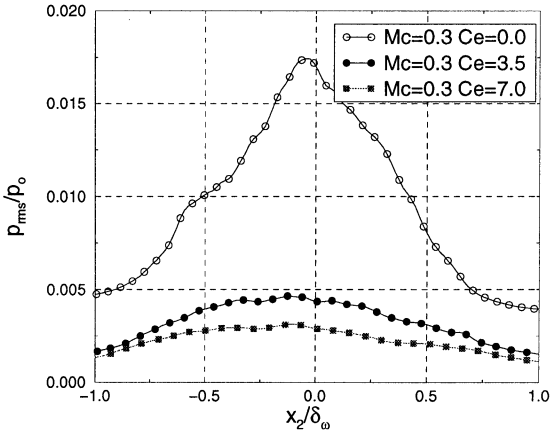

Figure 9: Pressure r.m.s. for different cases of heat release.